Annals of Biomedical Engineering, Vol. 33, No. 4, April 2005 (© 2005) pp. 531–544
DOI: 10.1007/s10439-005-2512-5

A Nonparametric Method for Analysis of Fluorescence Emission in Combined Time and Wavelength Dimensions

OLGA V. IVANOVA,[1,2] LAURA MARCU,[1,2,3] and MICHAEL C. K. KHOO[1]

[1]Department of Biomedical Engineering, University of Southern California, Los Angeles, CA 90089; [2]Biophotonics Research and Technology Development, Department of Surgery, Cedars-Sinai Medical Center, Los Angeles, CA 90048; and [3]Department of Electrical-Engineering, University of Southern California, Los Angeles, CA 90089

(Received 2 April 2004; accepted 11 October 2004)

Abstract—We report a method for accurate recovery of tissue intrinsic fluorescence emission characteristics, including fluorescence lifetimes and spectral profiles, from complex two-dimensional (spectro-temporal) emission waveforms. Most algorithms for analysis of fluorescence data address separately the characteristics of either spectral emission or fluorescence relaxation time. We developed a novel nonparametric analytical method that allows for identification and estimation of the intrinsic Fluorescent Impulse Response Kernel (FIRK) simultaneously in time and wavelength dimensions. Modeling of FIRK was based on the characteristics of spectro-temporal fluorescence waveforms. Due to the decaying behavior of the fluorescence, a linear combination of discrete Laguerre functions was used to model the fluorescence response in time. To address the large variability of spectral profiles of distinct fluorophores, a discrete Fourier series expansion was used to model the variation of fluorescence intensity across wavelength. The proposed method was validated on synthetic fluorescence data and data measured from fluorescence lifetime standards and tissue endogenous fluorescent biomolecules. We determined that this method provides a direct recovery of the two-dimensional FIRK and accurate estimation (residual error $<6\%$) of a broad range of fluorescence lifetimes including the sub-nanosecond range. The FIRK retrieved using this method can further facilitate modeling and recognition of pathological and physiological conditions in tissues.

Keywords—Fluorescent impulse response kernel, Time-resolved fluorescent spectroscopy, Two-dimensional system identification.

INTRODUCTION

Over the past few decades fluorescent spectroscopy has been widely explored as potential method for investigation and characterization of biological tissues.[1,3,6,12,21] The fluorescence signal remitted upon the interaction of excitation light with a biological sample contains information about sample biochemical content, metabolic status, microenvironment, and morphology. This information can be further used for characterization, diagnosis and monitoring of complex biological systems such as tissues and cells. The presence of several endogenous fluorophores, or intrinsic fluorescent bio-molecules in biological tissues, including amino acids (tryptophan, tyrosine), enzyme cofactors (nicotinamide adenine dinucleotide, flavin adenine dinucleotide), and structural proteins (elastin, collagen), offer the potential to directly probe the biochemical or metabolic changes in diseased tissues using fluorescence-based techniques.[6,18] For example, measurements of endogenous fluorescence have shown potential for diagnosis and staging of atherosclerotic plaques and tumors.[1,6,12,21] The fluorescence techniques, moreover, can enhance the specificity of conventional diagnostic imaging methods (ultrasound, magnetic resonance imaging, computer tomography) and enable the optimization of therapeutic procedures.

The fluorescence emission is measured using either steady-state or time-resolved techniques. Steady-state fluorescence techniques have been widely employed since they require a relatively simple and inexpensive instrumentation. However, the tissue fluorophores are characterized by a broad-band spectra that often overlap. Thus the emission spectra of distinct fluorophores are difficult to resolve when only steady-state techniques are used for investigation. The time-resolved approach involves measurements of the time-dependent properties of the fluorescent emission. The fluorescence lifetimes provide effective means of discrimination among fluorophores, as their spectrally overlapped signals are often characterized by distinct time-dependent intensity decays ranging from sub-picosecond to microsecond time scales.[6,18] The lifetimes are also sensitive to microenvironment (pH, temperature, enzymatic activity), thus lifetime measurements allow these parameters to be analyzed. Detection of small changes in the environment of fluorophores, for example, enables a better understanding of the metabolic activities within tissue and assessment of the diseased tissue response to therapy.

Address correspondence to Laura Marcu, PhD, Biophotonics Research Lab., Department of Surgery, Cedars-Sinai Medical Center, 8700 Beverly Blvd. Davis G149A, Los Angeles, CA 90048. Electronic-mail: lmarcu@bmsrs.usc.edu

Characterization and classification of tissues fluorescent response rely on selection of signal analysis techniques able to accurately reveal the true representation of the underlying fluorescence dynamics. Numerous analytical tools including least squares iterative reconvolution method,[2,33] method of moments,[28] along with Laplace[9] and Fourier[6] transform based techniques have been devised to retrieve the intrinsic fluorescent response of the sample. These methods have been widely applied in the field of fluorescence spectroscopy and thoroughly reviewed in the literature.[11,18,28] However, the common limitation of these methods is that they address separately the spectral and temporal profiles of an observed fluorescent phenomenon.

The composite biological structures may contain distinct fluorophores that simultaneously respond to external excitation, thus the resulting fluorescent output has a broad spectral profile and varying intensity decay kinetics along the emission spectrum. In this case the separate analysis of individual decay curves has been found usually insufficient and may result in loss of valuable information about competitive fluorescence processes in complex biological systems. Information that may be further used for characterization and identification of fluorescent systems. Consequently, for an accurate recovery of complex fluorescent decay phenomena it is advantageous to combine several fluorescent decay experiments into a single analysis.[4]

The widely applied signal-processing tool, based on the simultaneous analysis of multiple fluorescence decay experiments, is frequently referred to as "global analysis" approach.[4] This method relies on the physical modeling of the observed fluorescent phenomenon that is characterized by a set of fitting parameters invariant to different experimental settings. The error surface in global analysis was found to be much better defined than in the case of individual curve analysis due to the large number of experimental axes. Thus, the major advantage of the global analysis is that the fitting parameters of the physical model can be recovered with much smaller uncertainties than in individual curve analysis.[4]

In fluorescence-based diagnostic of tissues, however, it is often difficult to build the accurate parametric physical models of the intrinsic tissue fluorescence since there is a limited insight into the processes governing the fluorescent response of such complex biological samples.[35] In this case the researcher rather has the option of "black box" or nonparametric system identification method.[17] This method allows the derivation of an explicit mathematical expression that describes quantitatively the input–output functional relation from the observed input–output data. This approach provides the purely empirical identification of sample fluorescent properties and can serve as a foundation for further characterization and recognition of different tissue types.

The main goal of this study was to develop a nonparametric system identification method based on simultaneous estimate of FIRK in time and wavelength dimension that could be effectively used for the representation of complex fluorescent system such as biological tissues. In the following, we introduced mathematical concepts related to a two-dimensional (2-D) estimation method of the FIRK, and presented the validation of this analytical method on simulated fluorescence data and experimental data collected from various lifetime fluorescent standards and fluorescent biomolecules.

Because most fluorescent measurements data are analyzed using digital signal processing algorithms, the proposed identification method assumes discrete base and the FIRK $= H(nT, k\lambda)$. Experimental data used in current study was acquired using a pulse-sampling time-domain time-resolved technique (gated detection and fast digitizer).[21] This method has intrinsic advantages for *in vivo* measurements of tissue, including fast and direct recording of the time-resolved fluorescence intensity decay along the entire emission spectrum, and suitability for fiber optic or catheter type diagnostic systems.[8] Recording of variations in fluorescence intensity decay across emission spectrum allows recovery of the steady-state spectra by integrating the intensity decay signals, and provides a more complete description of the biochemical content, thus improving the specificity of fluorescence measurement.[1,2,21]

METHODS

Estimation Method for the Two-Dimensional Fluorescent Impulse Response Kernel

Mathematical Model

Upon tissue sample excitation with a pulsed light probe $X(nT, k\lambda)$ or input signal, fluorophores within tissue return to their ground state by emitting photons (fluorescence emission). For complex biological systems such as tissues, several fluorophores are likely to be excited simultaneously by a defined input light probe, however, each fluorophore will be characterized by specific fluorescent response. Therefore, to fully characterize the fluorescent emission of a tissue sample the temporal evolution of fluorescent pulse transient $Y(nT, k\lambda)$, or the output signal, is recorded across the entire spectrum of emission.[8]

Under this assumption, to determine the intrinsic FIRK one may employ a deconvolution method to separate input light probe signal from fluorescence output in the presence of system noise. We modeled this process as a 2-D single input–single output system that is characterized by the discrete convolution sum:

$$Y(nT, k\lambda) = \sum_{m=0}^{N-1} \sum_{l=K_0}^{K} H(mT, l\lambda) \cdot X(nT - mT, k\lambda - l\lambda) \cdot \times T \cdot \lambda + E(nT, k\lambda). \quad (1)$$

where the terms are defined as follow: $Y(nT, k\lambda)$, fluorescence output signal; $X(nT, k\lambda)$, input light probe;

$H(nT, k\lambda)$, fluorescent impulse response kernel; $E(nT, k\lambda)$, system error (noise); T, sampling interval in time; λ, sampling interval in wavelength; N, total number of data points in time dimension; K, wavelength in the spectrum.

The target function of interest is $H(nT, k\lambda)$. This function carries the empirical information about intrinsic fluorescent characteristics of the tissue, independent of the specific waveform of excitation, experimental apparatus and experimental conditions. The above model makes the assumption that the distortions to the fluorescent signal due to the light probe and data collection system are negligible or contribute only as an additive experimental noise.

A second assumption that we made was to assume that the sample contains non-interacting fluorophores resulting in a spectrally linear fluorescence response, and that superposition principle holds true. Physically this is equivalent to the process of weighted direct energy transfer from the input laser pulse emitted at certain wavelength into the fluorescent emission output at different wavelengths. In this case one can represent the 2-D FIRK as follow:

$$H(nT, k\lambda) = H_T(nT) \cdot H_\lambda(k\lambda). \tag{2}$$

where (nT) and $(k\lambda)$, independent variables for any n and k; $H_T(nT)$, impulse response kernel in discrete time space; $H_\lambda(k\lambda)$, impulse response kernel in discrete wavelength space.

The Basis Functions for Time and Wavelength Dimensions

The modeling of $H_T(nT)$ and $H_\lambda(k\lambda)$ was based on typical fluorescent signal profiles that are observed in the time and wavelength dimensions, respectively. Complete orthonormal families of functions were selected as basis of functions for both dimensions. This allows us to uniquely build FIRKs that can reconstruct fluorescent responses of arbitrary waveform.

Due to the exponentially decaying nature of the fluorescent response in time, for $H_T(nT)$ our basis of choice was the discrete Laguerre family of functions.[24,25] These functions have a built-in exponential term that makes them suitable for physical systems with exponential relaxation dynamics. The Laguerre kernel expansion basis has been extensively used for the modeling of the physiological processes.[20,22,25]

$$H_T(nT) = \sum_{i=0}^{X} C_i \cdot L_i(nT). \tag{3}$$

where $L_i(nT)$ is the discrete time Laguerre functions ($nT = \tau \geq 0$) defined as:

$$L_i(\tau) = \alpha^{(\tau-i)/2} \cdot \sqrt{1-\alpha} \sum_{k=0}^{i} (-1)^k \cdot \binom{\tau}{k} \cdot \binom{i}{k} \cdot \times \alpha^{i-k} \cdot (1-\alpha). \tag{4}$$

where C_i, unknown Laguerre coefficients; α, parameter that determines the rate of exponential decline of Laguerre functions; X, total number of Laguerre functions used for expansion.

The length of the kernel in time determines the memory of the system. The maximum length corresponds to the entire length of the signal output matrix in time; shorter lengths are more feasible for optimal computational performance since the intrinsic fluorescent decay is faster than the observed cumulative output. The optimal length of the kernel was determined using an optimization routine to produce the best-fit numerical model.

The intrinsic Laguerre parameter α was estimated based on the kernel length and number of Laguerre functions, and accepted when the value of highest order Laguerre function at the last point of the kernel was reduced to a level less than 5% of its absolute maximum. This produces computationally compact representation of kernel. The use of the discrete time Laguerre family of functions offers accurate kernel estimation from relatively short experimental data records in presence of data contaminating noise.[24] This is a very useful feature for modeling of fluorescent processes with fast decay kinetics in the sub-nanosecond range where the length of the experimental data record and therefore the resolution of the decay surface are limited by the currently available instrumental data acquisition rates.

Since the wavelength representation of $H_\lambda(k\lambda)$ reflects the spectral profile of the analyzed sample, it varies significantly with sample type. To address this variability, the discrete orthogonal Fourier series expansion was selected as basis for the wavelength dimension. Fourier series expansion is widely exploited in signal analysis and biomedical signal processing.[5,29] The discrete time Fourier series decomposes a discrete time signal into a sum of discrete time exponential functions:

$$H_\lambda(k\lambda) = \sum_{p=0}^{M-1} A_p \cdot \exp\left\{ jp\frac{2\pi}{M}k\lambda \right\} = \sum_{p=0}^{M-1} A_p \cdot F_p. \tag{5}$$

where A_p, unknown series coefficients; M, total number of data points in wavelength dimension.

To summarize, FIRK is written in the form:

$$H(nT, k\lambda) = \sum_{i=0}^{X} C_i \cdot L_i(nT) \sum_{p=0}^{M-1} A_p \cdot F_p(k\lambda). \tag{6}$$

where C_i and A_p are the unknown coefficients of Laguerre and Fourier functions.

To determine these coefficients we employed least-squares estimation procedure for the 2-D problem. This method is described in the subsequent section.

Least-Squares Estimation Procedure for the 2-D Problem

The nonlinear least-squares fitting methods based on the minimization of the chi-square statistic is the most popular approach for the analysis of fluorescence emission.[18,28] However, the use of chi-square function as a criterion for model selection requires additional assumptions regarding the statistics of residual data and experimental variance for the specific instrumentation used. Generally, it is implied that the measurement errors either follow the Gaussian distribution (or random noise signal) or Poissonian distribution (in single photon counting techniques). This approach is used in the analysis of fluorescent decays acquired with time correlated single photon counting (TCSPC) technique, the most commonly used method for acquiring time-resolved fluorescence data, where the statistical distribution of experimental noise is known.[27,28] If the error statistics deviates from Gaussian or Poissonian, the experimental variance has to be estimated or assumed prior to the analysis of decay curves. For the pulse-sampling time-resolved fluorescence spectroscopy technique, however, the measurement experimental variance is not known. Representative experimental data are needed to numerically evaluate the statistical distribution of experimental noise. This factor lead to an obvious problem of biased estimate of fluorescent impulse response[31,32] and can sometime mask important information contained in the model residual signal.

The least-squares minimization algorithm presented here allows for the best fit estimate by selecting the fluorescent impulse response kernel that would minimize the sum of squares of all the errors.[15] We made no assumption about the statistic of system noise, except that it is additive to the fluorescent output signal and the instrument does not introduce systematic errors. To practically implement the nonparametric model described above and calculate the coefficients of fluorescent impulse response kernel, we employed classical linear least-squares estimation technique. The advantage of this method is that the mathematical model can be written as a large but over-determined system of linear equations. The total number of the coefficients (unknown parameters) that is estimated is significantly less then the number of linear equations used in the analysis. In this case, the least-squares solution to the identification problem is unique. When the involved experimental signal has little or no experimental repeatability (statistics), as in case of fluorescence measurements *in vivo*, the over-determined system guarantees the unique solution and increases the confidence of the recovered model parameters.

To proceed, the 2-D convolution sum is restated in the matrix-vector format conventional for linear least-squares. Thus Eq. (1) is rewritten in the following form:

$$Y(nT, k\lambda) = \sum_{i=0}^{M-1} \sum_{p=0}^{X} D_{ip} \cdot G_{ip}(nT, k\lambda) + E(nT, k\lambda). \tag{7}$$

where $D_{ip} = C_i \cdot A_p$, coefficients to be estimated; $E(nT, k\lambda)$, noise; and $G_{ip}(nT, k\lambda)$ is defined as:

$$G_{ip}(nT, k\lambda) = \sum_{m=0}^{N-1} \sum_{l=0}^{K-1} L_i(nT) \cdot F_p(k\lambda) \cdot \times X(nT - mT, k\lambda - l\lambda) \cdot T \cdot \lambda; \tag{8}$$

The function $G_{ip}(nT, k\lambda)$ is determined by the experimental input data and choice of orthogonal basis functions in both time and wavelength dimensions.

Next, the summation in Eq. (7) was opened and the terms rearranged to fit the desired classical matrix-vector format:

$$\bar{Y} = G \cdot \bar{D} + \bar{E}. \tag{9}$$

where $\bar{Y}$, output vector; $\bar{D}$, vector of coefficients; $\bar{E}$, error vector; G, input matrix that are defined below as:

$$\bar{Y} = [\bar{Y}(0,0); \bar{Y}(0, 1 \cdot \lambda); \ldots \bar{Y}(0, (M-1) \cdot \lambda); \ldots \bar{Y}((N-1) \cdot T, 0); \bar{Y}((N-1) \cdot T, (M-1) \cdot \lambda)].$$

$$\bar{E} = [E(0,0); E(0, 1 \cdot \lambda); \ldots E(0, (M-1) \cdot \lambda); \ldots E((N-1) \cdot T, 0); E((N-1) \cdot T, (M-1) \cdot \lambda)].$$

$$\bar{D} = [D_{00}; D_{01}; \ldots D_{0x}; D_{10}; \ldots D_{M-1,0}; D_{M-1,1}; \ldots D_{M-1,x}].$$

$$G = \begin{pmatrix} G_{00}(0,0); \ldots G_{0x}(0,0); \ldots G_{M-1,0}(0,0); \ldots G_{M-1,x}(0,0) \\ G_{00}(0,\lambda); \ldots G_{0x}(0,\lambda); \ldots G_{M-1,0}(0,\lambda); \ldots G_{M-1,x}(0,\lambda) \\ \ldots \\ G_{00}((N-1)T, (M-1)\lambda); \ldots G_{M-1,x}((N-1)T, (M-1)\lambda) \end{pmatrix}. \tag{10}$$

The least-squares solution to the 2-D problem is given by the following equation:

$$\bar{D} = (G' \cdot G)^{-1} \cdot G' \cdot \bar{Y}. \tag{11}$$

Using the values from the vector of coefficients $\bar{D}$ the 2-D FIRK $H(nT, k\lambda)$ can be built.

Because acquisition of fluorescence data in clinical circumstances results in the lack of knowledge of the noise level for each data point, there is a need to estimate the experimental uncertainties during data analysis. In the case of no or very limited experimental statistics, the Cramer-Rao lower bound to the estimate[30] allows evaluation of the least minimal model error. We employed this method in this study. The Cramer-Rao lower bound to the estimate of the variance associated with the determined elements of $\bar{D}$ was calculated using the following formula:

$$\mathrm{var}(\bar{D}) = (G' \cdot G)^{-1} \cdot \sigma_e^2. \tag{12}$$

where σ_e^2 is the variance of the residual errors $E(nT, k\lambda)$. This is a lower bound on the precision that cannot be superseded.

One numerical requirement of obtaining the good estimates of $\bar{D}$ is that the matrix $(G' \cdot G)$ must not be singular or ill-conditioned, since it has to be inverted; otherwise the variance of the coefficient vector $\bar{D}$ will become infinite or very large. However, in real experimental applications there is a possibility to encounter the ill-conditioned data matrix and this situation requires special numerical treatment in order to reach the accurate and stable solution. The successful implementation of the model depends on the use of the developed robust numerical algorithms[7,13,16,17] that address the matrix inversion problem. In practice, we implemented the singular value decomposition method to ensure the stability of the solution.[31,32]

Goodness of the Fit Criteria

The use of the autocorrelation function to test for whiteness of the residuals is widely accepted as a method of merit for goodness of fit between model and experimental data in the signal analysis of various time-varying processes.[5,29] We replaced the classical goodness of fit test for single dimension autocorrelation function with the use of the 2-D autocorrelation function. This allows us to simultaneously check the randomness of the residual signal in both time and wavelength dimensions. The 2-D formulation of autocorrelation function, a commonly used method in optical information processing, digital image processing and image reconstruction, can be applied to any 2-D signal to test its randomness. Thus, the coefficients of 2-D autocorrelation matrix were calculated according to the formula:

$$R(m,l) = \sum_{n=0}^{N-m-1} \sum_{k=K_0}^{K-l} \frac{E(nT, k\lambda) \times E((n+m)T, (k+l)\lambda)}{(N-m-1)(K-l-K_0)}. \tag{13}$$

where m is the value of lag in time dimension; l the value of lag in wavelength dimension; $E(nT, k\lambda)$ the residual error signal; N the total number of data points in time dimension; K the wavelength in the spectrum.

The shape of the 2-D autocorrelation function of residuals may serve as criterion to test spectrally linear fluorescence response. To assess the extent of linearity of residual fluorescent signal by the means of 2-D autocorrelation test, the computational routine has to be established for calculation of 2-D confidence interval surfaces. Since the time-resolved pulse sampling fluorescence lifetime spectroscopy technique does not allow a direct estimation of the experimental noise statistics, this lack of knowledge about measurement uncertainty has to be addressed at the data analysis stage.[18,31] In this case, reference statistical parameters of the experimental uncertainties have to be estimated through the computing intensive statistical methods. In these methods, the observed data are used to generate the confidence intervals by means of randomization.[23] Randomization tests have several advantages, including flexibility and relative ease of implementation without distributional assumptions (e.g. Normal or Poisson). In our study, the confidence intervals for 2-D autocorrelation test were generated using the following randomization procedure.

First, we rearranged the order of the model residual errors $E(nT, k\lambda)$ over the entire time–wavelength matrix of the signal by shifting them randomly; second, the 2-D autocorrelation function of the residual errors was computed. Those steps are repeated many times (e.g. 100 or more) and the results were saved to generate large data set of autocorrelation tests. Then, we computed the statistic of each data point on the 2-D autocorrelation matrix with results forming the standard deviation matrix. The average value of standard deviation σ was calculated over the standard deviation matrix and was used to generate the reference confidence interval surfaces for 2-D autocorrelation test.

Coupling the 2-D autocorrelation test with evaluation of the level of residual errors allowed us to assess the relative contribution from linear and nonlinear parts of the signal into the cumulative intrinsic fluorescent output, thus to estimate the extent of sample's spectrally linear fluorescence response. This analysis cannot be performed using only time-dependent fluorescent signal processing routines, since these routines implicitly assume spectrally linear behavior of the analyzed fluorescent sample, thus making the proposed 2-D system identification technique a feasible fluorescent system diagnostic tool.

Another criterion to monitor the adequacy of model fit to the experimental data was time-integrated fluorescent spectrum for experimental and reconstructed signals that correspond to conventionally measured steady-state fluorescent spectrum along the region of fluorescent emission.

Optimization Criterion

When recovering the fluorescent impulse response kernel $H(T, k\lambda)$ from experimental noisy signal the reduction of the total number of model coefficients while keeping the adequate model fit is essential for producing a computationally economical and compact routine.

The total number of model coefficients and their optimal values depend on the set of the adjustable parameters of our model. These parameters include the total number of Laguerre and Fourier basis functions used and the length of the kernel in time dimension (due to the time-dependent behavior of the fluorescence intensity). As a criterion for optimization purposes we used the least-squares error function J (the weighted sum of squares of the difference between the data values and the model estimated values) calculated for each initial adjustable model parameter set.

$$J = \frac{1}{(N-K)\cdot(K-K_0)} \cdot \sum_{n=0}^{N-1} \sum_{k=K_0}^{K} \{Y_{\text{exp}}(nT, k\lambda) - Y_{\text{est}}(nT, k\lambda)\}^2 \tag{14}$$

The minimum value of error function J corresponds to the optimal initial model parameter set that allows achieving the optimal mean-square approximation of the system output. Where $Y_{\text{experimental}}(nT, k\lambda)$ and $Y_{\text{estimated}}(nT, k\lambda)$ are the corresponding measured and reconstructed fluorescent output computed using the convolution of estimated fluorescent impulse response kernel $H(nT, k\lambda)$ with input laser pulse $X(nT, k\lambda)$.

All computations were performed with the software package MATLAB® (The MathWorks, Natick, MA).

Algorithm for Validation

Validation on Synthetic Data: Prove of Unique Solution

The efficacy of the proposed system identification approach is illustrated below using computer-simulated fluorescent signals. The synthetic fluorescent output was constructed to emulate the model output. First, we generated the FIRK $H_{\text{model}}(nT, k\lambda)$ using Laguerre and Fourier functions (Eqs. (7)–(10)), then the simulated FIRK was convolved with the input laser pulse $X_{\text{model}}(nT, k\lambda)$ to create a synthetic fluorescent output signal $Y_{\text{model}}(nT, k\lambda)$. The simulated data set contained observations at exactly the same independent variables, i.e. time and wavelength axes, as the original signal.

To represent experimental system uncertainties, the simulated data set was contaminated by additive synthetic 'random noise.' The additive synthetic random noise was generated by means of randomization[23] using the experimentally measured system noise. Then, the order of experimentally measured system noise was rearranged over the entire time–wavelength matrix of the signal by shifting the values randomly and ensuring that the statistical descriptors (the mean and the variance) remain the same as for measured system noise. This is to satisfy our initial assumption that the distortions to the fluorescent signal due to the light probe and data collection system are negligible or contribute only as an additive experimental noise. Thus, the generated synthetic fluorescent signal $Y_{\text{model+noise}}(nT, k\lambda)$ is in conformity to all assumptions made above in the development of system identification method and serves as a test signal for algorithm validation (Fig. 1(a)).

The synthetic fluorescent data was used to prove that the proposed algorithm for the estimation of FIRK yields a unique solution. First, the 'noise containing' synthetic fluorescent output signal was processed to obtain the corresponding FIRK $H_{\text{model+noise}}(nT, k\lambda)$. Second, the 'noise free' synthetic fluorescent output signal was processed using the same set of adjustable parameters as the 'noise containing' synthetic fluorescent output signal. The residual signal was calculated between the two fluorescent impulse response kernels $H_{\text{model}}(nT, k\lambda)$ and $H_{\text{mode+noisel}}(nT, k\lambda)$. The value of residual error function J for compared FIRK signals is in the order of 10^{-15} that is at the level of digitization error of the computing system. We concluded that the 'noise free' FIRK is a 100% fit to FIRK from synthetic 'noise containing' signal as demonstrated by the zero level of residual values, thus proving the unique solution to the system identification problem.

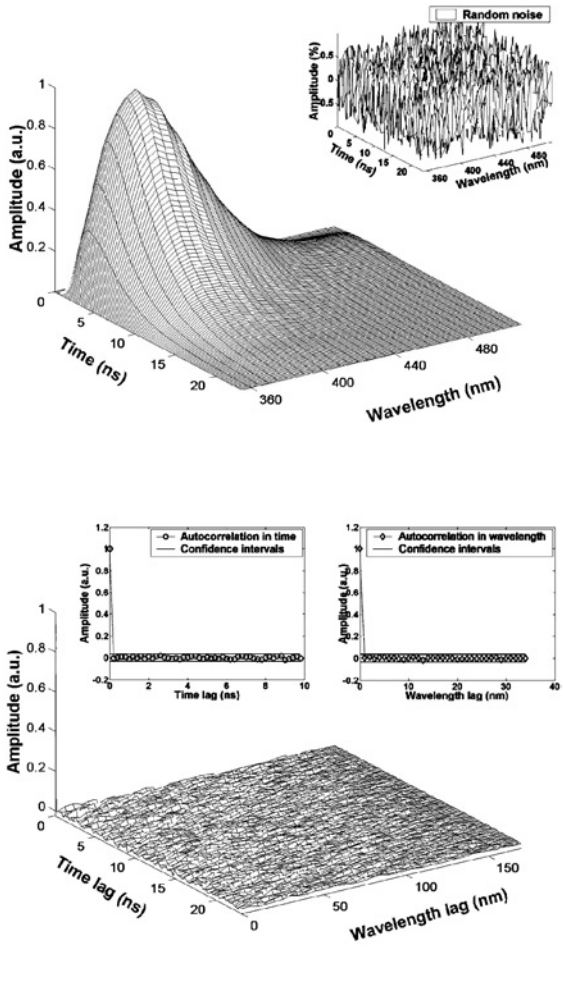

FIGURE 1. (a) Synthetic fluorescent output signal. Inset: additive random noise; (b) results of the 2-D autocorrelation test for model residual errors. Insets: 2-D autocorrelation (time, left panel; wavelength, right panel).

Validation of Synthetic Data: Analysis of Residuals

The performance of the 2-D autocorrelation test was evaluated for the ideal case, when the synthetic fluorescent data is contaminated by the additive random noise $Y_{\text{model+noise}}(nT, k\lambda)$ as mentioned above. This data served as fluorescent output and used for retrieval of FIRK and further reconstruction of model signal $Y_{\text{model}}(nT, k\lambda)$. The residual data matrix between the synthetic 'noise containing' signal $Y_{\text{model+noise}}(nT, k\lambda)$ and reconstructed model signal $Y_{\text{model}}(nT, k\lambda)$ was analyzed using a 2-D autocorrelation test. Before the application of autocorrelation test, the mean of the residual matrix was calculated and subtracted from

each data point on the residual surface to create zero mean signal since mean shift model could also result in autocorrelation between the values.

The resultant autocorrelation matrix is shown in Fig. 1(b). Because the autocorrelation matrix is a symmetrical matrix only one quadrant is displayed. This matrix presents the autocorrelation coefficients between each pair of the residual errors $E(nT, k\lambda)$ matrix. The diagonal elements of this matrix correspond to the correlation between each residual data point. The center of the matrix represents the autocorrelation with zero lags in both time and wavelength and is unity by definition (normalized autocorrelation). The observed result exhibit the single non-zero peak at zero lag in both time and wavelength dimensions. This is the ideal case autocorrelation result that we can achieve with our model on spectrally linear synthetic data.

Validation on Solutions of Fluorescence Lifetime Standards

Time-resolved fluorescence data were collected from fluorescence lifetime standards using a compact fiber-based fluorescent spectroscopy apparatus for *in situ* time-resolved laser-induced fluorescence spectroscopy of tissue.[8] The following fluorophores were used in this study: 9-cyanoanthracene in ethanol; Rose Bengal in both ethanol and methanol; Rhodamine B in both ethanol and in DI water; and mixture of 9-cyanoanthracene/Rhodamine B mixture in ethanol.

The fluorescence emission was induced with a pulsed nitrogen laser (337.1 nm emission wavelength, 1.2 ns pulse width), measured in the spectral range from 360 to 700 nm (5 nm wavelength increment) and digitized with 5 GSamples/s sampling frequency. To improve the signal to noise ratio, each recorded fluorescence pulse transient (output signal) consisted of an average of 16 consecutive fluorescence pulses. Scattered laser pulse (input signal) was measured at wavelengths below 337 nm. Experimental noise was measured at 400 nm after the samples were removed. For signal processing the collected experimental data were arranged into a two-dimensional matrix format (wavelength, time) for both input and output signals.

Since the experimental input signal is very narrow and contains only laser line at 337 nm, it had to be zero padded to span the same wavelength-time space as the collected fluorescent output. To minimize the contribution of experimental noise to the output signal, the mean value of experimental noise signal was subtracted from the analyzed data before the estimation of the FIRK, $H(nT, k\lambda)$. The experimental data collected from the fluorescence standards was used to demonstrate that our mathematical method and its numerical implementation do not introduce any artifacts into calculated FIRK and allows the effective recovery of the fluorescence time-decay constants.

Performance of the Deconvolution Technique: 1-D Laguerre Expansion of Kernels vs. 2-D Laguerre-Fourier Expansion of Kernels

The performance of the fluorescent system identification method developed in this study was evaluated by comparing the variability of fluorescence lifetimes along the emission spectrum retrieved with our method (2-D analysis) with that obtained using the conventional approach for time-dimension only (1-D analysis). For 1-D analysis the fluorescence impulse response function is retrieved separately for each wavelength using an algorithm based on the first order Laguerre expansion of kernels.[16,20] For each fluorophore, the lifetime variability was evaluated for every wavelength in the emission spectrum. For single fluorophore solutions, the estimated spectral mean and standard deviation of lifetime values were calculated across the spectrum of emission using both 1-D and 2-D analysis. For the 9-cyanoanthracene/Rhodamine B mixture solution, the estimated spectral mean and standard deviation of lifetime values were calculated across the spectrum of emission of each individual fluorophore (the spectra overlap is minimal). In both cases all initial input system parameters were kept identical.

RESULTS

Validation on Solutions of Fluorescent Lifetime Standards

The average lifetime value was estimated as the time at which the FIRK $H(nT, k\lambda)$ decays to $1/e$ of its maximum

TABLE 1. Lifetime (τ) values for fluorescent standard solutions.

Sample	Solvent	Peak λ (nm)	2-D $H(nT, k\lambda)$ τ(ns)	1-D literature[10,19] τ (ns)	Spectral range λ (nm)	2-D spectral mean $\tau \pm$ SD (ns)	1-D spectral mean $\tau \pm$ SD (ns)
9/CA	Ethanol	440	11.31	11.85	370–520	12.78 ± 0.55	12.81 ± 0.69
Rhodamin B	Ethanol	580	2.76	2.85	510–650	2.73 ± 0.16	2.88 ± 0.41
Rhodamin B	DI water	580	1.60	1.52	510–650	1.70 ± 0.18	2.19 ± 0.32
Rose Bengal	Ethanol	580	0.90	0.85	530–650	0.79 ± 0.15	0.89 ± 0.34
Rose Bengal	Methanol	575	0.62	0.54	530–650	0.61 ± 0.12	0.68 ± 0.22
9CA$*$ /Rhodamin B$**$ Mix	Ethanol	440	10.73	11.85	410–520	9.74 ± 0.41	9.78 ± 0.53
9/CA	Ethanol	580	2.98	2.85	540–650	2.67 ± 0.18	2.95 ± 0.30

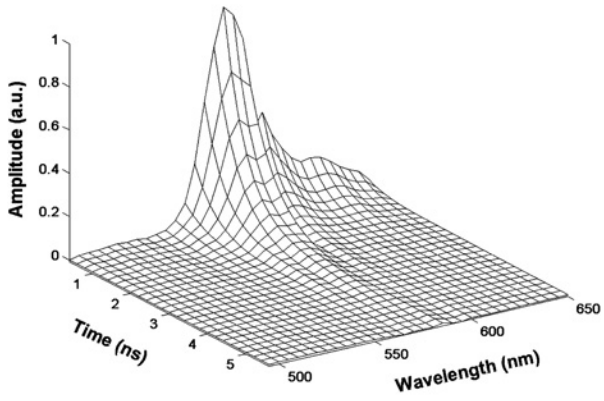

(a)

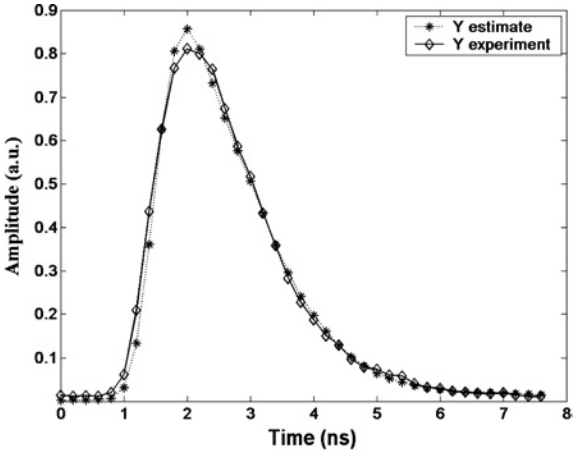

(d)

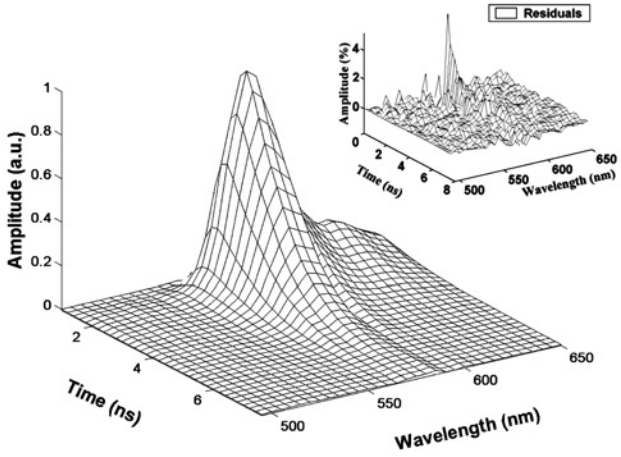

(b)

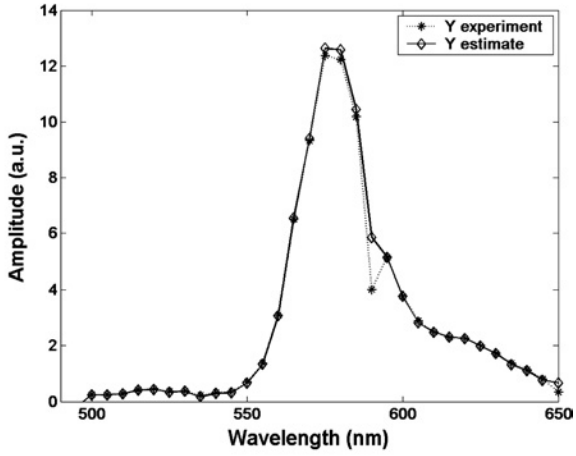

(e)

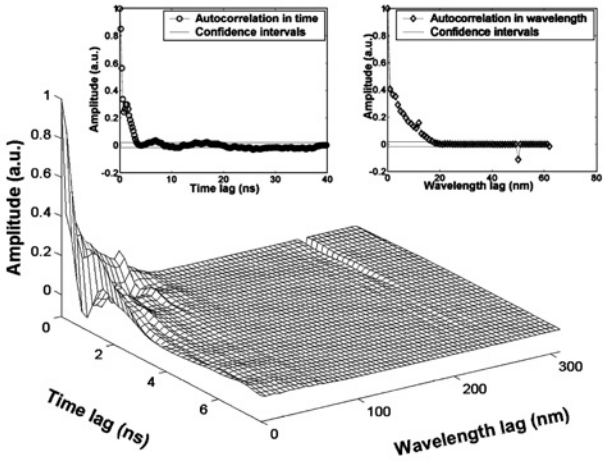

(c)

FIGURE 2. Results for Rose Bengal in 10^{-6} M ethanol solution. (a) FIRK. (b) Model reconstruction of fluorescent signal. Inset: residual errors between model and experimental fluorescent outputs. (c) 2-D autocorrelation function of residuals. Insets: 2-D autocorrelation function (time, left panel; wavelength, right panel). (d) Time decay profile at peak emission wavelength 575 nm. (e) Steady-state emission spectra.

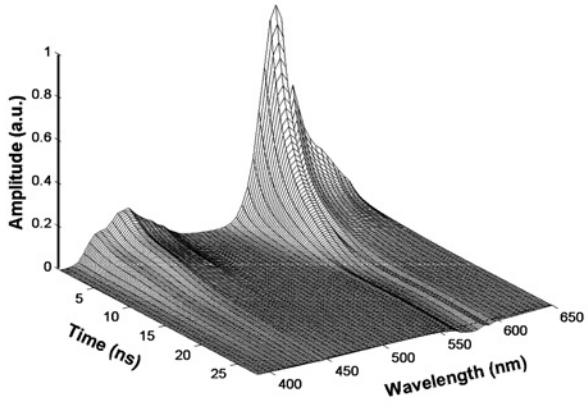

(a)

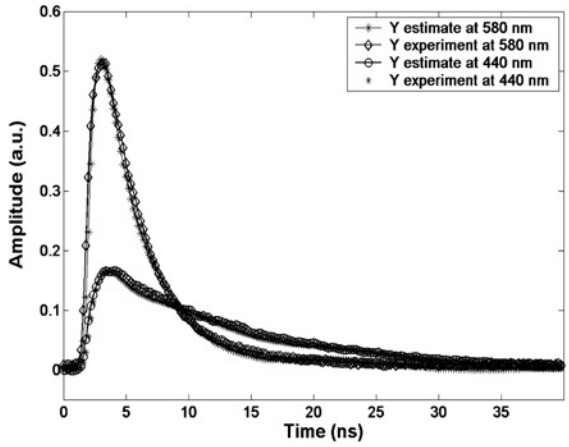

(d)

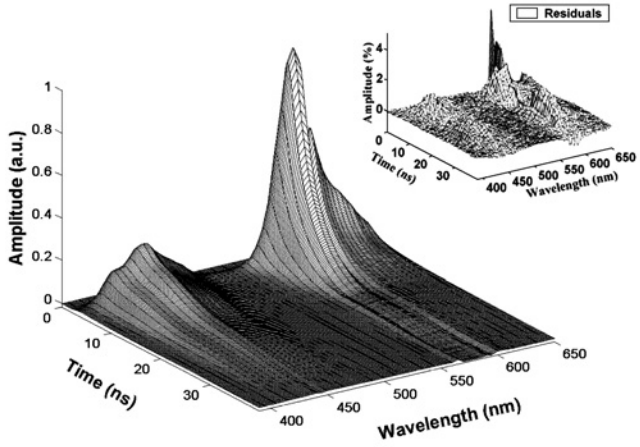

(b)

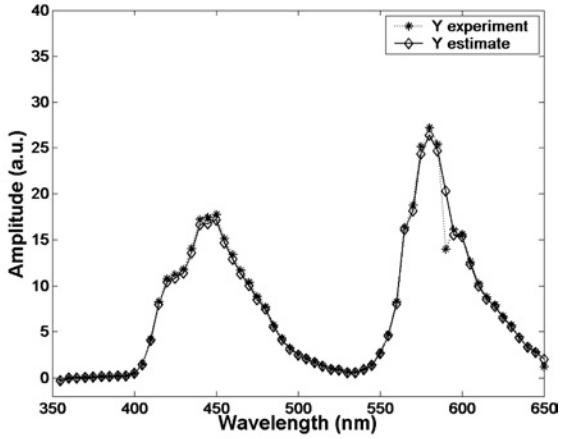

(e)

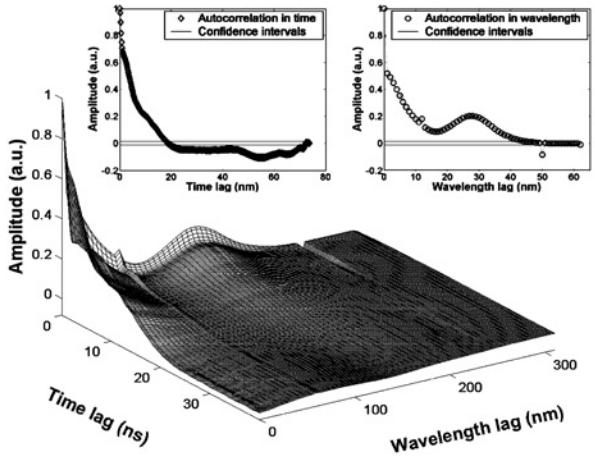

(c)

FIGURE 3. Results for a 5×10^{-6} M solution of 9-cyanoanthracene and Rhodamin B mixture dissolved in ethanol. (a) FIRK. (b) Model reconstruction of fluorescent signal. Inset: residual errors between model and experimental fluorescent outputs. (c) 2-D autocorrelation function of residuals. Insets: 2-D autocorrelation function (time, left panel; wavelength, right panel). (d) Time decay profile at peak wavelength 580 and 440 nm Model reconstructed fluorescent signal ± SE and experimental fluorescent signal. (e) Steady-state spectra. Model reconstructed fluorescent signal ± SE and experimental fluorescent signal.

intensity. The lifetime values for fluorescent standards retrieved using our method were found in agreement with those reported in the literature.[10,18,19] The fluorescence lifetimes for each component at main peak emission are summarized in Table 1. Figure 2 depicts the results for Rose Bengal in ethanol, a fluorescent probe with very fast decay kinetics (lifetime below 1 ns).

To illustrate the potential of current algorithm to resolve simultaneously the complex fluorescence emission of a mixture of fluorophores, we applied the algorithm to fluorescence data acquired from a mixture of two fluorescent standards in solution: 9-cyanoanthracene (short-lived) and Rhodamine B (long-lived) in ethanol. The relative concentration of Rhodamine B in mixture is 50%. The estimated FIRK are presented in Fig. 3.

For all reported cases, we evaluate the level of residual errors (Table 2). The maximum, mean and standard deviation values of residual errors were given in percentages to the maximum normalized intensity of the measured fluorescent signal. For example, in the case of the mixture of two fluorescent standards in solution the mean value of residual errors is 4.5% and residual errors do not exceed 6.2% of the maximum measured fluorescent output signal. For all reported cases, the residual signals were found to not exceed 6.5% of the maximum fluorescence intensity output signal. The residual errors were further tested for whiteness using the 2-D autocorrelation test. Results for Rose Bengal solution and mixture solutions are displayed in Figs. 2 and 3. Comparison of the 2-D autocorrelation surfaces of residual errors from experimental fluorescent data with ideal case 2-D autocorrelation surface from synthetic data suggests a remaining nonrandom informational content left. This is an important observation indicating that sample fluorescence cannot be fully described by the linear model employed in this work. However, the level of residual error allows us to estimate the relative contribution from linear and nonlinear parts of the signal into the cumulative intrinsic fluorescent output, thus to estimate the extent of sample spectral linearity (Table 2).

Performance of the 1-D vs. 2-D Deconvolution Technique on the Mixture of Fluorescent Standard Solutions

The mean lifetime values for 9CA/Rhodamin B mixture in solution and Rose Bengal in ethanol are presented in Fig. 4; the spectral ranges and the mean lifetimes ± standard deviation for each fluorescent standards are given in Table 1.

TABLE 2. Residual values for fluorescent standard solutions.

Sample	Solvent	Residual errors $E(nT, k\lambda)$ (%) Max	Mean	SD
9/CA	Ethanol	6.10	5.30	2.09
Rhodamin B	Ethanol	5.90	5.05	1.89
Rhodamin B	DI water	6.07	4.80	1.03
Rose Bengal	Ethanol	6.01	5.90	1.71
Rose Bengal	Methanol	5.15	4.80	1.20
9CA/Rhodamin B Mix	Ethanol	6.20	4.50	1.92

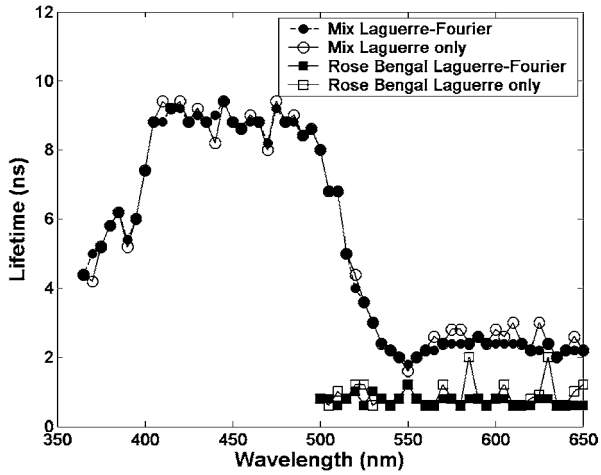

FIGURE 4. The 1-D and 2-D estimated fluorescence lifetime values for fluorescent standard solution of 9-cyanoanthracene and Rhodamin B mixture in ethanol and Rose Bengal in ethanol.

In each case, the values of standard deviation were found smaller for 2-D FIRK estimation when compared to 1-D approximation. These results suggest that the application of the 2-D approach results in less variability in lifetime values across the spectrum of emission as compared 1-D method, thus yielding a more robust lifetime estimate. This demonstrates that the proposed 2-D system identification method is less sensitive to the variations in noise level across the emission spectrum. The noise contamination can severely influence the accuracy of retrieving the true fluorescent lifetimes. This is especially important for the estimation of the decay dynamics measured from mixture of fluorescent components with overlapping spectra or short-lived fluorophores (lifetimes <2 ns). Accurate measurements of short-lived fluorescence are more likely to depend on the time-resolution of the experimental system. The larger the number of data points acquired along the decay curve the more accurate estimation of fluorescence lifetimes can be achieved.

Application to Experimental Data from Fluorescent Biomolecules

In this section we present results from the FIRK estimation conducted on the fluorescent output from samples of major endogenous tissue fluorescent biomolecules including elastin and distinct types of collagen. The five fluorescent tissue specimens tested in this study include commercially available samples (Sigma-Aldrich) of elastin, collagen type I from tendon, collagen type I from calf skin, collagen type II from cartilage and collagen type V from placenta.

The fluorescence lifetime values of the fluorescent bio-molecules were retrieved using the 2-D system

TABLE 3. Lifetime values for fluorescent bio-molecules.

Sample	Peak λ (nm)	2-D $H(nT, k\lambda)$ τ (ns)	1-D literature[20,21] τ (ns)	Residual errors $E(nT, k\lambda)$ (%)		
				Max	Mean	SD
Elastin Ligament	420	1.8	1.3	5.87	4.50	1.10
Collagen I Tendon	440	2.42	3.9	5.90	4.10	2.08
Collagen I Calf Skin	435	0.92	—	6.15	5.70	1.80
Collagen II Cartilage	390	3.10	—	5.10	4.83	1.15
Collagen V Placenta	430	0.60	—	6.02	5.40	0.90

identification method described in this study. The lifetime values at peak emission spectrum are displayed in Table 3. These values were found in agreement with those reported in the literature for these molecules.[20,21] The applicability of the algorithm is illustrated on time-resolved spectra collected from samples of collagen II that is characterized by slow decay kinetics (Fig. 5). The remaining residual errors are within 6% of the maximum value of fluorescence intensity (Table 3), although the 2-D autocorrelation tests exhibit a well-defined non-random pattern. The low level of residual errors suggests that the fluorescence emission of these fluorescent biomolecules can be well described within our basic model assumptions.

DISCUSSION

In this study, we used a linear combination of discrete Laguerre functions combined with a discrete Fourier series expansion to model the profile of fluorescence emission. The fluorescence intensity decay (time-dimension) was fitted to a maximum of eight Laguerre functions. This number of functions was found sufficient for providing an accurate signal reconstruction and kernel estimation for both fluorescence lifetime standards in solutions and endogenous fluorescent molecules in tissues. The variation of fluorescence intensity across spectrum (wavelength-dimension) was approximated using a number of discrete Fourier basis functions that equal the total number of wavelengths for each fluorescent component. The modeling results are reported assuming a linear response of fluorescent sample in response to a pulsed light stimulus.

Our results demonstrated that the 2-D implementation of FIRK estimation provides a accurate estimate of fluorescent response of biological samples, provided that experimental conditions satisfy the basic model assumption. The samples with significant nonlinear fluorescence response would likely exhibit large value of residual errors in our best-fit estimate. For the reported cases, we achieved a low level of residual signal that does not exceed 6% of the maximum normalized fluorescence intensity output indicating a relative linear fluorescence response of analyzed samples in response to light stimulus. However, further analysis of the 2-D autocorrelation suggested that there is a residual information content not attributed by our model.

Additionally, should the researcher encounter such a biological system with significant nonlinearities, our technique can be further expanded to incorporate these nonlinear effects of energy transfer from light excitation pulse to the fluorescent biological sample by employing the higher orders of the Laguerre expansion kernels and adding the nonlinear signal processing blocks to the current model. Such a diagnostic test is not possible to be perform with traditionally 1-D deconvolution techniques, since they entirely rely on the assumed linear behavior of the system. In this case, the problem has to be addressed either with additional experiments on the representative sample type, or by employing the certain model of interaction between the light radiation and biological matter. Both scenarios can reduce the accuracy of system identification and increase the complexity of experimental investigation.

Another useful feature is that the selection of basis expansion functions for time and wavelength dimensions is merely a researcher choice and can be easily tailored to observed phenomena with the rest of the mathematical framework intact. This option may allow for the more compact signal processing routines that are application specific and computationally effective. The two dimensional single-input single-output framework of the algorithm allows to identify the intrinsic fluorescence parameters of a sample excited with virtually any input light probe spatio-temporal profile. Therefore, the investigator is not limited to the use of only narrow band short laser pulse to probe the fluorescent sample, but also can employ the complex spatio-temporal light input signal, i.e. the simultaneous coherent excitation at different wavelengths, train of laser pulses or broadband pulsed ultraviolet light sources, etc., depending upon application. Such an approach not only can yield more information about the studied specimen but also enables simplification of the entire experimental setup.

CONCLUSION

An important feature of time-resolved fluorescence data is its multidimensional nature intensity vs. wavelength vs. time. The system identification method presented in this study allowed for the simultaneous analysis of the multidimensional fluorescence decay surface by taking into account the spectral and temporal aspects of fluorescence emission output with just a few basic and general

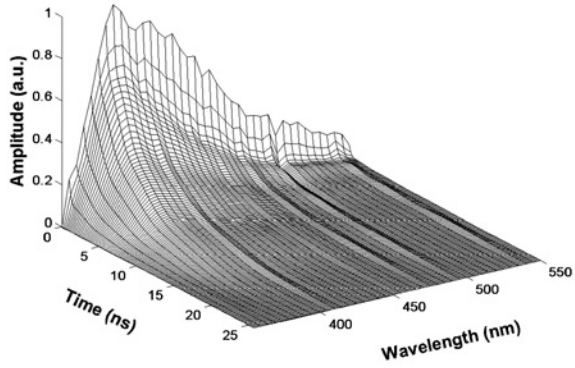

(a)

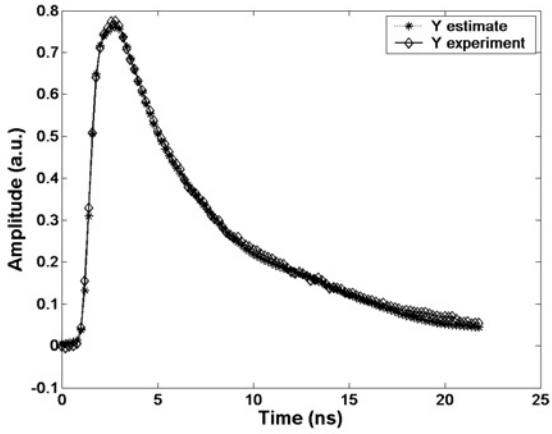

(d)

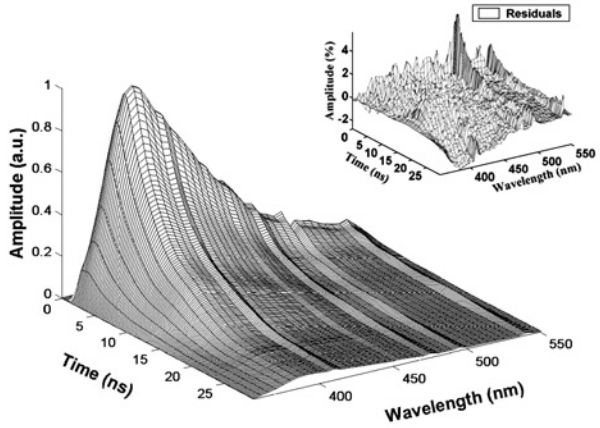

(b)

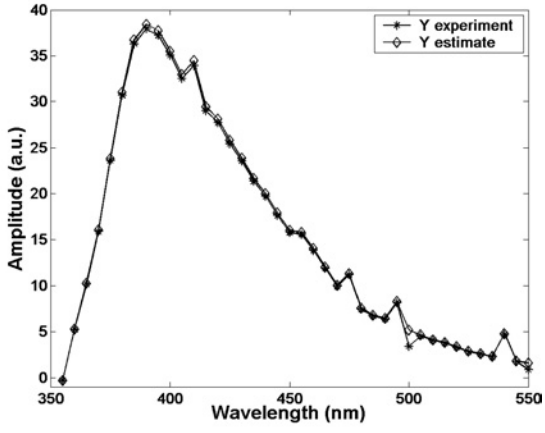

(e)

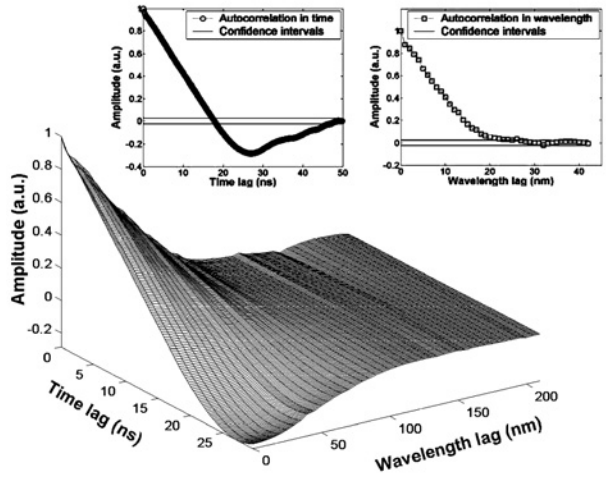

(c)

FIGURE 5. Results for Collagen type II. (a) FIRK. (b) Model reconstruction of fluorescent signal. Figure insert: (a) Residual error between model and experimental fluorescent outputs. (b) Model reconstruction of fluorescent signal. Inset: residuals between model and experimental fluorescent outputs. (c) 2-D autocorrelation function of residuals. Insets: 2-D autocorrelation function (time, left panel; wavelength, right panel). (d) Time decay profile (displayed at peak wavelength 380 nm). Model reconstructed fluorescent signal ± SE and experimental fluorescent signal. (e) Steady-state spectra. Model reconstructed fluorescent signal ± SE and experimental fluorescent signal.

assumptions made about the light probe/fluorescent sample interactions and experimental system conditions. This provides reliable and accurate recovery of the intrinsic fluorescent parameters of the investigated sample from the measured cumulative fluorescent output as illustrated with data from fluorescent standard solutions and fluorescent biomolecules.

This study supports previously reported evidence[4,18,33] that for complex fluorescent systems it is advantageous to consider simultaneous analysis of fluorescent decay data. How does the nonparametric identification of optical fluorescent system in combined time and wavelength spaces relate to another multidimensional global analysis[4] approach? The application of nonparametric, or "black box" system identification method to analysis of fluorescence intensity decay from biological samples do not dependent on the physical model of the observed fluorescent phenomenon, and thus allows expansion of the intrinsic fluorescent response of any form without a priori assumption of its spatio-temporal profile. This characteristic makes this method suitable for applications where little or no information is available to build an accurate parametric physical model of intrinsic fluorescence. In contrast, the use of parametric global analysis[4] for system identification purposes will require such information and thus the applicability of such technique is limited. The presented nonparametric approach, however, shares the major advantages of global analysis by employing the same concept of global error that is much better defined than in individual curve analysis due to the large number of experimental axes. The same concept of overdetermination of fluorescent system is realized through the use of the direct least-squares implementation in combined time and wavelength dimensions. When the involved experimental signal has little or no experimental repeatability (statistics) as in case of *in vivo* fluorescence measurements the over-determined system guarantees the unique solution and increases the confidence of the recovered model parameters, thus solving the identifiability problem. The estimated FIRK can be further examined for modeling and classification of pathological and physiological conditions of tissues. This approach shows potential for development of reliable optical diagnostic methods that take advantage of advances in non-parametric system identification techniques.

ACKNOWLEDGMENTS

This work was supported in part the National Institute of Health (R01 HL 67377-01), the Whitaker Foundation (RG-01-0346), and the Biomedical Simulations Resource at the University of Southern California. We would like to thank Dr. Qiyin Fang for providing the experimental data for this study. The authors are grateful to Prof. Robert Kalaba and Prof. Vasilis Marmarelis for useful discussions.

REFERENCES

[1] Andersson-Engels, S., J. Johansson, and S. Svanberg. The use of time-resolved fluorescence for diagnosis of atherosclerotic plaque and malignant tumors. *Spectrochim. Acta* 40A:1203–1210, 1990.

[2] Badea, M., and L. Brand. Time resolved fluorescence measurements. *Methods Enzymol.* 61:378–425, 1979.

[3] Baraga, J. J., P. Taroni, Y. D. Park, K. An, A. Maestri, L. L. Tong, R. P. Rava, C. Kittrell, R. R. Dasari, and M. S. Feld. Ultraviolet laser induced fluorescence of human aorta. *Spectrochim. Acta* 45:95–99, 1989.

[4] Beechem, J. M., E. Gratton, M. Ameloot, J. R. Knutson, and L. Brand. The global analysis of fluorescence intensity and anisotropy decay data: Second-generation theory and programs. In: Topics in Fluorescence Spectroscopy, edited by J. R. Lakowicz. New York: Plenum Press, 1991, pp. 241–305.

[5] Bruce, E. N. Biomedical Signal Processing and Signal Modeling. New York: Wiley Series in Telecommunications and Signal Processing, 2001.

[6] Cubeddu, R., D. Comelli, D. C. D'Andrea, P. Taroni, and G. Valentini. Time-resolved fluorescence imaging in biology and medicine. *J. Phys. D: Appl. Phys.* 35:61–76, 2002.

[7] Faddeev, D. K., and V. N. Faddeeva, Computational Methods of Linear Algebra. San Francisco: W.H. Freeman, 1963.

[8] Fang, Q., T. Papaioannou, J. A. Jo, R. Vaitha, and K. Shastry. Time-domain laser-induced fluorescence spectroscopy apparatus for clinical diagnostics. *Rev. Sci. Instrum.* 75:151–162, 2004.

[9] Gafni, A., R. L. Modlin, and L. Brand. Analysis of fluorescent decay curves by means of the Laplace transformation. *Biophys. J.* 15:263–280, 1975.

[10] Grinvald, A. The use of standards in the analysis of fluorescence decay data. *Anal. Biochem.* 30:261–279, 1976.

[11] Grinvald, A., and I. Z. Steinberg. On the analysis of fluorescence decay kinetics by the method of least squares. *Anal. Biochem.* 59:583–598, 1974.

[12] Glanzmann, T., J. P. Ballini, H. van den Bergh, and G. Wagnieres. Time-resolved spectrofluorometer for clinical tissue characterization during endoscopy. *Rev. Sci. Instrum.* 70:4067–4077, 1999.

[13] Golub, G. H., and C. F. Van Loan. Matrix Computations. Baltimore: The Johns Hopkins University Press, 1983.

[14] Jo, J. A., Q. Fang, T. Papaioannou, and L. Marcu. Fast model-free deconvolution of fluorescence decay for analysis of biological systems. *J. Biomed. Opt.* 9(4):743–752, 2004.

[15] Khoo, M. Physiological Control Systems: Analysis, Simulation and Estimation. New York: IEEE Press Series in Biomedical Engineering, 2000.

[16] Kalaba, R. E., and N. Rasakhoo. Algorithms for generalized inverses. *J. Opt. Th. Appl.* 48:427–435, 1986.

[17] Kalaba, R. E., and K. Springarn. Control, Identification and Input Optimization. New York: Plenum Press, 1982.

[18] Lakowicz, J. R. Principles of Fluorescent Spectroscopy, 2nd ed. New York: Kluwer Academic/Plenum, 1999.

[19] Lampert, R. A., L. A. Chewter, and D. Phillips. Standards for nanosecond fluorescence decay time measurement. *Anal. Chem.* 55:68–73, 1983.

[20] Maarek, J. M. I., L. Marcu, W. J. Snyder, and W. S. Grundfest. Time-resolved fluorescence spectra of arterial fluorescent compounds reconstruction with Laguerre expansion technique. *Photochem. Photobiol.* 71:178–187, 2000.

[21] Marcu, L., M. C. Fishbein, J. M. Maarek, and W. S. Grundfest. Discrimination of human coronary artery atherosclerotic lipid-rich lesions by time-resolved laser-induced fluorescence spectroscopy. *Atheroscl. Thromb. Vasc. Biol.* 21:1244–1250, 2001.

[22]Marcu, L., W. S. Grundfest, and M. C. Fishbein. Time-resolved laser-induced fluorescence spectroscopy for staging atherosclerotic lesions. In: Fluorescence in Biomedicine, edited by M. A. Mycek, and B. Pogue. New York: Marcel Dekker, 2003, pp. 397–430.
[23]Manly, B. F. J. Randomization, Bootstrap, and Monte Carlo Methods in Biology. New York: Wiley, 1997.
[24]Marmarelis, V. Z. Identification of nonlinear biological systems using Laguerre expansion of kernels. *Ann. Biomed. Eng.* 21:573–589, 1993.
[25]Marmarelis, V. Z. Modeling methodology for nonlinear physiological systems. *Ann. Biomed. Eng.* 25:239–251, 1997.
[26]McGown, L. B. Fluorescence lifetime filtering. *Anal. Chem.* 61:839–847, 1989.
[27]O'Connor, D. V., and D. Phillips. Time-Correlated Single Photon Counting. London: Academic Press, 1984.
[28]O'Connor, D. V., W. R. Ware, and J. C. Andre. Deconvolution of fluorescence decay curves. A critical comparison of techniques. *J. Phys. Chem.* 83:1333–1343, 1979.
[29]Proakis, J. G., and D. G. Manolakis. Digital Signal Processing. Principles, Algorithms, and Applications. Upper Saddle River: Prentice Hall, 1996.
[30]Proakis, J. G. Digital Communications, 4th ed. McGraw-Hill, 2001.
[31]Stavridi, M., V. Z. Marmarelis, and W. S. Grundfest. Spectro-temporal studies of Xe–Cl excimer laser induced arterial wall fluorescence. *Med. Eng. Phys.* 17:595–601, 1995.
[32]Tellinghuisen, J., and C. W. Wilkerson, Jr. Bias and precision in the estimation of exponential decay parameters from sparse data. *Anal. Chem.* 65:1240–1246, 1993.
[33]Vallotton, P., and R. Vogel. Parameter recovery in frequency-domain time-resolved fluorescent spectroscopy; resolution off the prototropic forms of 5-carboxyfluorescein in the physiological pH range. *J. Fluoresc.* 10:325–332, 2000.
[34]Ware, W. R., L. J. Doemeny, and T. L. Nemzek. Deconvolution of fluorescence and phosphorescence decay curves. A least squares method. *J. Phys. Chem.* 77:2038–2048, 1973.
[35]Webb, S. E. D., Y. Gu, S. Leveque-Fort, J. Siegel, M. J. Cole, K. Dowling, R. Jones, and P. M. W. French. A wide-field time-domain fluorescence lifetime imaging microscope with optical sectioning. *Rev. Sci. Instrum.* 73:1898–1907, 2002.